Science Bulletin 65 (2020) 1607–1613

Contents lists available at ScienceDirect

Science Bulletin

journal homepage: www.elsevier.com/locate/scib

Science Bulletin
www.scibull.com

Article

A selective control of volatile and non-volatile superconductivity in an insulating copper oxide via ionic liquid gating

Xinjian Wei [a,b], Hao-Bo Li [c], Qinghua Zhang [a], Dong Li [a,b], Mingyang Qin [a,b], Li Xu [a,b], Wei Hu [a,b], Qing Huan [a], Li Yu [a], Jun Miao [d], Jie Yuan [a,e], Beiyi Zhu [a], Anna Kusmartseva [f], Feo V. Kusmartsev [f], Alejandro V. Silhanek [g], Tao Xiang [a,b], Weiqiang Yu [h], Yuan Lin [i], Lin Gu [a,b], Pu Yu [c], Qihong Chen [a,*], Kui Jin [a,b,e,*]

[a] Beijing National Laboratory for Condensed Matter Physics, Institute of Physics, Chinese Academy of Sciences, Beijing 100190, China
[b] School of Physical Sciences, University of Chinese Academy of Sciences, Beijing 100049, China
[c] State Key Laboratory of Low Dimensional Quantum Physics and Department of Physics, Tsinghua University, Beijing 100084, China
[d] State Key Laboratory for Advanced Metals and Materials, School of Materials Science and Engineering, University of Science and Technology Beijing, Beijing 100083, China
[e] Songshan Lake Materials Laboratory, Dongguan 523808, China
[f] Department of Physics, Loughborough University, LE11 3TU Loughborough, UK
[g] Experimental Physics of Nanostructured Materials, Q-MAT, CESAM, Université de Liège, B-4000 Sart Tilman, Belgium
[h] Department of Physics, Renmin University of China, Beijing 100872, China
[i] State Key Laboratory of Electronic Thin Films and Integrated Devices & Center for Information in Medicine, University of Electronic Science and Technology of China, Chengdu 610054, China

ARTICLE INFO

Article history:
Received 18 December 2019
Received in revised form 24 April 2020
Accepted 14 May 2020
Available online 19 May 2020

Keywords:
Parent cuprate
Electron-doped copper oxide
Superconducting thin film
Ionic liquid gating
Volatile and non-volatile superconductivity

ABSTRACT

Manipulating the superconducting states of high transition temperature (high-T_c) cuprate superconductors in an efficient and reliable way is of great importance for their applications in next-generation electronics. Here, employing ionic liquid gating, a selective control of volatile and non-volatile superconductivity is achieved in pristine insulating $Pr_2CuO_{4\pm\delta}$ (PCO) films, based on two distinct mechanisms. Firstly, with positive electric fields, the film can be reversibly switched between superconducting and non-superconducting states, attributed to the carrier doping effect. Secondly, the film becomes more resistive by applying negative bias voltage up to − 4 V, but strikingly, a non-volatile superconductivity is achieved once the gate voltage is removed. Such phenomenon represents a distinctive route of manipulating superconductivity in PCO, resulting from the doping healing of oxygen vacancies in copper-oxygen planes as unravelled by high-resolution scanning transmission electron microscope and *in situ* X-ray diffraction experiments. The effective manipulation of volatile/non-volatile superconductivity in the same parent cuprate brings more functionalities to superconducting electronics, as well as supplies flexible samples for investigating the nature of quantum phase transitions in high-T_c superconductors.

1. Introduction

Copper oxide (cuprate) superconductors continue to be considered as technologically attractive materials mainly due to their high transition temperature (high-T_c). Although high-T_c cuprate superconductors have been discovered for more than three decades, the micro mechanism still remains unclear and the progress of their applications in superconducting electronics is relatively slow. The superconductivity of cuprates is commonly achieved by doping charge carriers, via either cation substitution or oxygen variation, to the parent compound known as Mott insulator [1,2]. However, the superconductivity and physical properties of cuprates are very sensitive to subtle changes of chemical composition, which is hard to control during the synthesis procedure [3–5]. Lately, much effort was spent on controlling the superconducting properties via a two-step post-annealing method, which tunes the oxygen content and induces superconductivity in the insulating parent cuprates [6–8]. Such annealing process is performed at several hundred degrees Celsius, where only one superconducting state can be obtained in each trial, consequently the cost is high and the efficiency is low. Exploring an efficient *in situ* method to manipulate the superconductivity of cuprates will not only help us understand the origin of superconductivity in high-T_c superconductors, but also further promote their practical applications.

Lately, ionic liquid gating (ILG) technique emerged as an attractive method to trigger phase transitions by tuning the charge

* Corresponding authors.
E-mail addresses: qihongchen@iphy.ac.cn (Q. Chen), kuijin@iphy.ac.cn (K. Jin).

https://doi.org/10.1016/j.scib.2020.05.013
2095-9273/

carriers in a large scale (10^{14}–10^{15} cm^{-2}) with the electrostatic field effect [9–14]. For example, ILG can turn semiconducting ZrNCl [15] and MoS_2 [16] into superconductors, and tune the superconducting properties of $La_{2-x}Sr_xCuO_4$ [17], $YBa_2Cu_3O_{7-\delta}$ [18], $Pr_{2-x}Ce_xCuO_4$ [19,20], $La_{1.95}Ce_{0.05}CuO_4$ [21], and FeSe [22]. Such process is reversible as the gating effect vanishes after removing the gate voltage. In addition to the electrostatic field effect, some studies argue that electrochemical interactions driven by ILG, e.g., (de-)oxygenation and protonation, play an important role in driving materials into new electronic phases. This happens, for example, in oxides $SrCoO_{2.5}$ [23], VO_2 [24], $SrTiO_3$ [25] and in superconductors $La_{1.96}Sr_{0.04}CuO_4$ [26], $YBa_2Cu_3O_{7-\delta}$ [27,28], $NdBa_2Cu_3O_{7-\delta}$ [20], FeSe [29]. Nevertheless, in ionic liquid gated high-T_c superconductors, the microscopic pictures of oxygenation or protonation remain largely unknown. The complex interplay between electrostatic carrier doping and electrochemical reaction needs to be elucidated in order to understand the origin of high-T_c superconductivity. Therefore, it is tempting to systematically study the effect of ILG on high-T_c cuprates, by both electrostatic carrier doping and electrochemical interaction, which can be *in situ* controlled and thus will provide more device functionalities and better understanding of high-T_c superconductivity.

For this purpose, a prototypical parent cuprate $Pr_2CuO_{4\pm\delta}$ (PCO) is chosen as our model system. It consists of alternatively stacked fluorite-like rare earth layers and square-planar CuO_2 layers. PCO becomes superconducting by either electron injection with Ce doping, namely $Pr_{2-x}Ce_xCuO_4$, or carefully tuning the oxygen content via an annealing process, with a superconducting dome indicated by the blue region in Fig. 1a [30–32]. Therefore, this system provides an ideal platform for studying high-T_c superconductivity via ILG. We find that a positive gate voltage (PGV) can drive the insulating PCO thin films into superconducting state, forming a dome-like superconducting phase in the temperature-voltage (*T*-*V*) phase diagram (SC I in Fig. 1a), mimicking the superconducting dome in the phase diagram of *T*-Ce substitution [3]. Such a superconducting state disappears as the PGV is withdrawn, consistent with the previous reports on $La_{2-x}Ce_xCuO_4$ (LCCO) [21] and $Pr_{2-x}Ce_xCuO_4$ [19]. This phenomenon is interpreted as electron injection into the sample through the PGV process (see Fig. 1b).

Strikingly, although the sample becomes more resistive with a negative gate voltage (NGV) of −4 V, a non-volatile superconducting state emerges after the NGV is removed. A corresponding superconducting dome feature (SC II in Fig. 1a) via this NGV operation is presented in the *T*-*V* phase diagram along with the SC I dome. Combined with high-resolution scanning transmission electron microscope (HR-STEM) and *in situ* X-ray diffraction (XRD) measurements, we propose that the repairing of oxygen vacancies in the CuO_2 planes under the NGV process (see Fig. 1c) is a good candidate to understand such a new phenomenon.

2. Experimental methods

2.1. Sample preparation

PCO thin films were grown on [0 0 l]-oriented $SrTiO_3$ (STO) substrates by the polymer assisted deposition method. Firstly, the precursor solution was prepared by mixing Pr/Cu nitrates, polyethylenimine (PEI) and ethylenediaminetetraacetic acid (EDTA) in deionized water, as described in Ref. [32]. The precursor solution was first spin-coated on STO substrates and calcined at 550 °C in air to remove the organic residues. Successively, the as-grown samples were fired at 850 °C in a multizone tubular furnace with oxygen pressure of ~200 Pa for crystallization. Finally, these samples were annealed at 400–600 °C under an oxygen pressure of 1 Pa. By adjusting the annealing temperature and duration, insulating and superconducting samples with various T_c's were obtained. The typical film thickness is about 60 nm.

To check the structure and crystallinity of the PCO films, we performed the 2θ-scan and reciprocal space mapping (RSM) of the (−1 0 9) diffraction peak of the samples using XRD. The results are shown in Fig. S1a (online). All Bragg peaks can be indexed to (0 0 l) orientation, indicating that the film is in a single phase

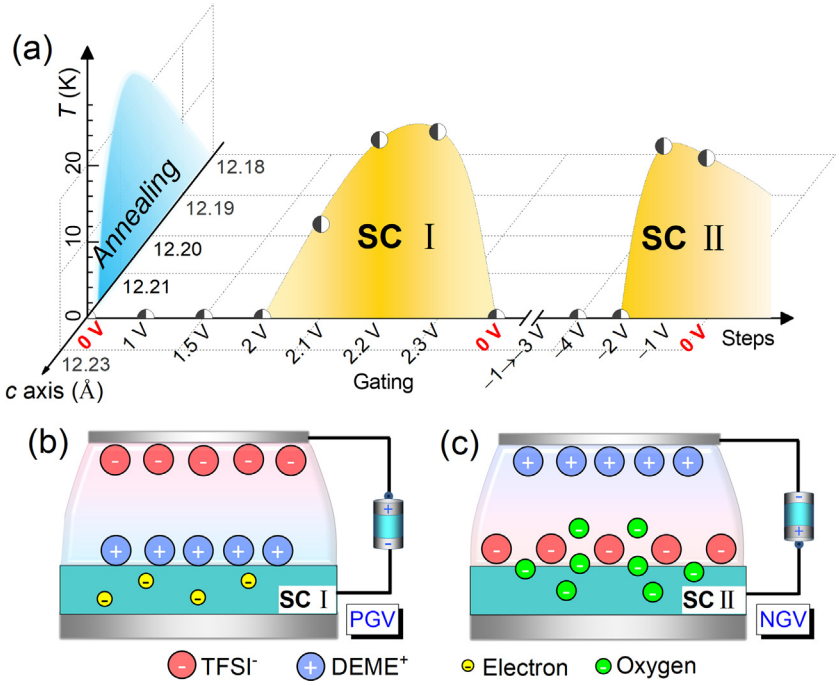

Fig. 1. (Color online) Phase diagrams of annealing and gating in $Pr_2CuO_{4\pm\delta}$. (a) The dependence of the superconducting transition temperature (T_c) as a function of the *c*-axis lattice constant (the blue dome) and gate voltages (yellow domes, SC I and SC II). The blue and yellow domes are obtained with the annealing and gating methods, respectively. (b, c) Schematic illustrations of electron carrier doping and oxygen vacancy repairing induced by ILG. (b) shows the configuration of the positive field gating by which the SC I dome arises and (c) shows negative field gating where the electrochemical reaction may occur, leading to the SC II dome.

with *c*-axis orientation. In addition, the RSM data in Fig. S1b (online) reveals that the PCO film has a good epitaxy.

2.2. Sample characterization

We carried out electrical transport measurements in the commercial physical property measurement system (PPMS). PCO samples were placed at the bottom of a small quartz-glass cup and immersed entirely by ionic liquid, as shown in Fig. S2 (online). A Pt slice as gate electrode was fixed to the side wall of the quartz-glass cup, which was mounted on the PPMS puck and transferred to PPMS. The electrical transport properties were measured with the internal electronic measurement system of PPMS, and an external Keithley 2400 source meter was employed to apply bias voltages between the sample and the gate electrode. All the samples were patterned into standard Hall bars. The electrodes were protected by GE varnish to avoid corrosion by electrochemical reaction. *In situ* XRD measurements were performed in a high-resolution diffractometer (SmartLab, Rigaku) with monochromatic Cu $K_{\alpha 1}$ radiation (λ = 1.5406 Å). The gate voltage varies from −2.5 to 2.5 V in steps of 0.5 V. Since the gating device shields the lower angle, the scanning 2θ range was set between 41° and 49°.

The micro-structure was investigated by the HR-STEM (ARM-200CF from JEOL) equipped with double spherical aberration (Cs) correctors. The PCO specimens were prepared by the focused ion beam technique and observed along the [1 1 0] zone axis. The experiments were performed at 200 keV and the probe current of angular bright-field (ABF) images and spectrum images (SI) were set at 23 and 68 pA, respectively, to avoid beam damage. The SI data was collected with a rate of 0.1 s/pixel and the energy dispersion for SI was set at 0.25 eV/pixel to obtain a high signal-to-noise ratio. The collection semi-angle in the electron energy loss spectroscopy (EELS) was 100 mrad.

3. Results and discussion

3.1. Volatile superconductivity with positive gate voltage

Fig. 2a shows the temperature dependence of resistance measured under various PGVs for sample S1. With increasing PGV (gating temperature T_g = 250 K), the normal state resistance gradually decreases and the sample becomes superconducting when PGV reaches 2.1 V. However, this superconductivity disappears once PGV is switched off. To detect the variation of carrier density with gating, we carried out Hall resistivity measurements. As can be seen in Fig. 2c, the Hall resistivity ρ_{xy} gradually increases with increasing PGV, similar to the effect of substituting Pr^{3+} by Ce^{4+} from underdoped regime to optimal doping [33,34]. This suggests that the PGV-induced superconductivity (SC I) is caused by electron doping, which is further supported by the gating experiment on another sample S2. As shown in Fig. 2e, S2 is originally superconducting and PGV can push the superconducting state into a metallic state, mimicking the superconductor-to-metal transition from optimally doped to heavily overdoped regime in Ce-doped PCO [1]. Therefore, by starting with only two different sample states (insulating and superconducting), the superconducting state tuned by ILG can span the whole phase diagram from underdoped to overdoped regime, in analog to electron doping by Ce-substitution.

Several possible effects, such as electrostatic charge modulation [15,16], oxygen removal [28,35], and H^+ ions injection [23,36–38] may arise during the PGV process in the oxide system. Considering the fact that the thickness of the PCO thin film, ~60 nm, is much larger than the Thomas-Fermi screening length (several nanometers), pure electrostatic field effect can only modulate the electronic property of the surface layers, and therefore cannot extend to the whole film and suppress the superconductivity of the bulk.

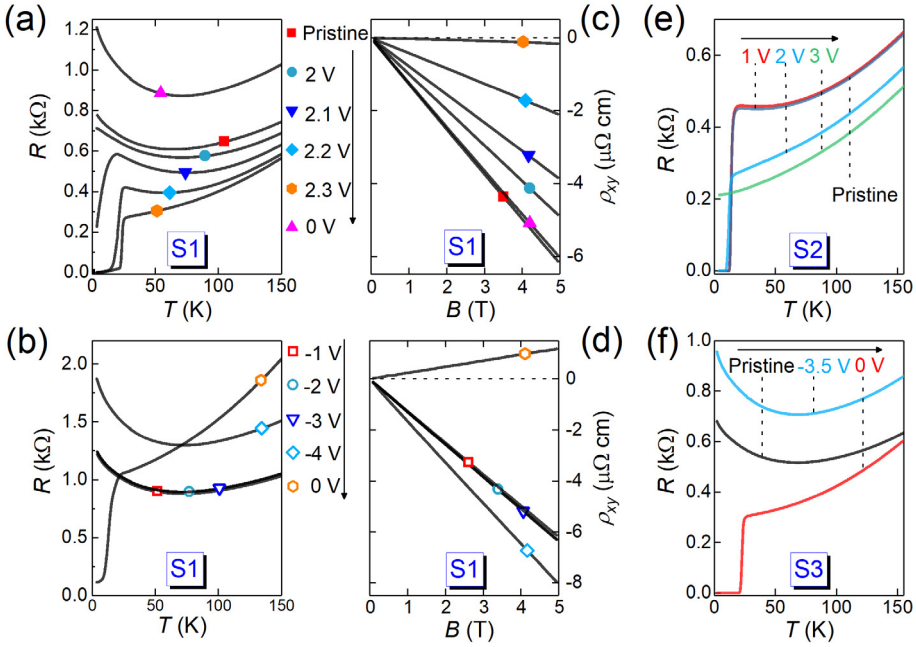

Fig. 2. (Color online) Electrical transport properties of PCO thin films under ILG. (a, b) Temperature dependence of resistance for sample S1 at various gate voltages, with gating sequence marked by the arrow. (a) demonstrates the volatile superconductivity with PGV process, where the superconductivity vanishes after retracting gate voltage. After gating, the resistance is higher than the original value, indicating the presence of electrochemical reaction. (b) shows the non-volatile superconductivity with NGV process, where superconductivity emerges after a gating cycle to −4 V and returning to 0 V. (c, d) Hall resistivity versus magnetic field measured at 30 K, corresponding to the gating states of panels (a) and (b), respectively. (e, f) Resistance as a function of temperature at different gate voltages for samples S2 and S3, respectively. For a superconducting sample S2, PGV can push the superconducting state into a metallic state. For a non-superconducting sample S3, directly applying and withdrawing NGV can also induce superconductivity, demonstrating the non-volatile superconductivity does not depend on PGV process. For all the experiments, the gating temperature is 250 K.

This conclusion is further substantiated by a contrast experiment with gating temperature lowered to 220 K, where the gating effect is purely electrostatic and the electrochemical reaction can be unambiguously excluded [15,16]. At T = 220 K, even by applying a V_g up to +3 V, no superconductivity occurs. When the gating temperature is raised to 250 K and the gate voltage reaches +2.1 V, PCO becomes superconducting immediately (Fig. S3 online). Therefore, pure electrostatic field effect can be ruled out. The deoxygenation effect is a more complex issue. In the next section, we will show that the negative gating process repairs the oxygen vacancies and induces superconductivity. Consequently, if the deoxygenation effect dominates the PGV process, more oxygen vacancies will be generated and the sample would be driven further away from the superconducting state. Therefore, although it might be present, deoxygenation should be a minor effect and cannot be responsible for the superconductivity induced in the PGV process. Instead, H^+ injection/removal is the most plausible explanation [29]. Our recent work has also proven H^+ injection/removal as the main mechanism to tune the superconductivity in another electron-doped cuprate LCCO [38]. H^+ ions locate at interstitial positions, and go out once the gate voltage is withdrawn.

3.2. Non-volatile superconductivity with negative gate voltage

In the negative bias gating process, as seen in Fig. 2b, the resistance of sample S1 shows an indiscernible change in the voltage range from 0 to −3 V (i.e., resistance curves almost overlap) whereas a remarkable increase occurs at −4 V. Surprisingly, a superconducting state emerges after the gate voltage is turned off. Correspondingly, the Hall resistivity barely changes in the voltage range from 0 to −3 V but drops substantially at −4 V, as illustrated in Fig. 2d. When the gate voltage is removed, there is an abrupt sign change of Hall resistivity from negative to positive. A similar phenomenon has been observed in $Pr_{2-x}Ce_xCuO_4$ with increasing Ce doping concentration from underdoped to overdoped regime [33,34]. However, a simple scenario based on electrostatic carrier doping cannot account for the nature of non-volatile superconductivity because the cycle of 0 → −4 → 0 V is unlikely to cause an electron doping effect. In other words, the superconducting phase SC II arises from a novel and peculiar effect, which is different from the PGV-driven deoxygenation or proton injection in copper- and iron-based superconductors [28,29,35]. In order to further verify that the SC II phase appearing after a cycle of NGV is indeed non-volatile, we did the measurements on another non-superconducting sample S3. As shown in Fig. 2f, superconductivity also emerges after the sample undergoes a NGV process to −3.5 V. A natural question one may ask is: what happens to the samples as the NGV reaches a threshold?

Previous studies demonstrate that NGV above a threshold could trigger an electrochemical reaction in some oxides, such as $SrCoO_{2.5}$ [23] and $YBa_2Cu_3O_{7-x}$ [28]. That is, oxygen ions are introduced into the samples. In order to get an explicit picture of the non-volatile superconductivity we observed, *in situ* XRD measurements were performed on an insulating PCO thin film at room temperature. As shown in Fig. 3, the almost unchanged full width at half maximum (FWHM, Fig. 3b) and angle (Fig. 3c) of (0 0 6) Bragg peak suggest minute crystallographic or structure factor modification along the *c*-axis in the ILG process. This also indicates that no extra oxygen ions are introduced to the apical sites, otherwise the *c*-axis lattice constant should increase [39,40]. Notably, the amplitude of (0 0 6) Bragg peak is significantly enhanced as the NGV is set to −2.5 V, highlighted by the red lines in Fig. 3a and red symbols in Fig. 3d. Such enhancement is retained after the gate bias is switched off, implying irreversible modification of the XRD form factor. In other words, the atomic electron density distribution and crystal structure change within the building block CuO_2 planes by negative voltage operation. Here the room temperature (~293 K) threshold bias voltage for NGV operation is about −2.5 V for the *in situ* XRD measurements. According to the NGV experiments performed at different gating temperatures, the threshold voltage for inducing superconductivity decreases with increasing temperature. At room temperature, the threshold voltage of −2.5 V is also consistent with the V_g-T_g parameter space for electrochemical interaction [41,42] (Fig. S4 online).

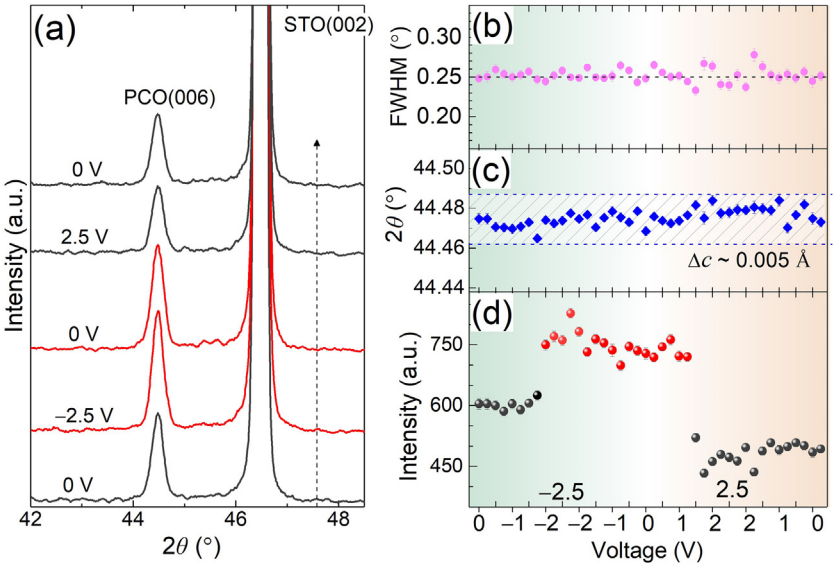

Fig. 3. (Color online) *In situ* XRD characterization of PCO thin films on $SrTiO_3$(0 0 1) substrates under ILG. (a) 2θ-scans at representative gate voltages. The curves are vertically shifted for clarity and the arrow with dotted line represents the ILG sequence. The 2θ-scans are measured with a voltage step of 0.5 V, and the time interval for each curve is about 14 min. The reference diffraction peak of the STO substrate remains almost unvaried during the gating process. (b–d) Gate voltage dependence of the full width at half maximum (FWHM) (b), angle (c) and amplitude (d) of PCO (0 0 6) peak. FWHM and angle have no changes during the whole gating process, as indicated by the dashed line in (b) and the shaded area in (c). $\Delta c \sim 0.005$ Å indicates the variation of *c*-lattice constant corresponding to the fluctuation of the diffraction angle. The amplitude of (0 0 6) peak significantly increases as the NGV reaches −2.5 V, marked in red color both in (a) and (d), and it weakens after switching to PGV. The measurement was performed at room temperature.

In order to identify the origin of such crystallographic and/or electronic related changes in the compound, we compare the HR-STEM and EELS results between superconducting (SC) and non-superconducting (NSC) samples. Fig. 4a and b are the ABF images with atomic resolution along the [1 1 0] zone axis for NSC and SC samples, respectively. The images have been processed by averaging multiple frames with the SmartAlign software [43], which are more representative and insensitive to noise. The dark, gray and light spots represent Pr, Cu and O, respectively, as indicated by the structure model overlaid on the upper right corner. Fig. 4d and e display the corresponding line profiles of CuO_2 layers in the atomic columns highlighted in Fig. 4a and b. The valleys correspond to the dark spots in the ABF image, where deeper valleys signify higher occupancy of oxygen or copper. Therefore, the content of oxygen can be reflected by the depth of the valleys marked with the inverted triangles (O atomic positions). The lines that connect the triangles of the NSC sample are much more undulating than that of the SC sample, suggesting that the oxygen atoms are not uniformly distributed in the NSC samples. Namely, more oxygen vacancies exist in the NSC sample. Furthermore, the oxygen *K*-edge spectra of EELS from both NSC and SC samples are presented in Fig. 4f. It is clear that the superconducting sample has a more pronounced leading edge peak structure in the EELS spectra, mainly related to the oxygen *p*-orbital hybridizing with the Cu *d*-orbital upper Hubbard branch from the CuO_2 planes [44]. Especially the major peak features around absorption threshold between 530 and 560 eV in the SC sample show clear spectroscopic distinction compared to the NSC sample. To be more specific, the peak feature around 535 eV presents clear red shift compared to its counterpart in the NSC spectra, and the peak around 545 eV pops out more pronouncedly from the spectral background in the SC sample. All these suggest clear electronic structure modification associated with oxygen ions in the CuO_2 planes induced by the NGV process.

It is known that unavoidable water inside the ionic liquid can decompose into negatively charged O^{2-} and positively charged H^+ through electrolysis if sufficiently high gate voltage is applied [23,38]. Under NGV, anions accumulate on the surface of the sample. Since the oxygen vacancies in CuO_2 planes actually act as positively charged centers, they will attract negatively charged oxygen ions O^{2-} once the electrostatic potential can overcome the crystal lattice energy. Therefore, it is reasonable to speculate that the −3.5 V bias plays a role in repairing the oxygen vacancies electrochemically within the CuO_2 planes, and consequently alters some local electron density distribution, which is consistent with the variation of peak amplitude in the *in situ* XRD measurements.

3.3. Discussion

Finally, we discuss possible mechanisms for the non-volatile superconductivity. Considerable oxygen vacancies in CuO_2 planes act as potential barriers, breaking Cooper pairs and preventing the pristine samples from showing superconductivity [45]. It is known that there exists a charge transfer gap between the upper Hubbard band (Cu $d_{x^2-y^2}$ orbit) and the O 2*p* band in cuprates [46]. The charge transfer gap can be smeared out by chemical doping [47] or field effect doping [48], due to the enhanced Coulomb screening effect and weakened on-site Coulomb repulsion [49]. It should be pointed out that the non-superconducting PCO samples used here for ILG are not ideal Mott insulators, but rather slightly doped insulators with Mottness. At the bias voltage −4 V, on the one hand, the electrochemical reaction process reduces oxygen vacancies in the CuO_2 plane and thus the pair-break scattering decreases; on the other hand, the conduction carrier density decreases due to the reduction of oxygen vacancies and thus the charge transfer gap is substantially enhanced, causing a sharp decrease of Hall resistivity and the absence of superconductivity. Once the gate voltage returns from −4 to 0 V, the charge transfer gap turns to close, thereby allowing the emergence of superconductivity. Since electrons and holes come from the upper Hubbard band and O 2*p* band, respectively, the mixture of these two bands results in the coexistence of two-type carriers. Such speculation can explain the non-linear magnetic field dependence of Hall resistivity as the NGV is removed, but requires that hole-type carriers dominate the transport for a positive Hall resistivity (Fig. 2d). Another possibility is that besides the replenishing of oxygen vacancies, some oxygen ions are introduced to the interstitial sites, meanwhile bringing hole-type carriers into the film. Withdrawing the electric field, the interstitial oxygen ions accumulate near the film surface, resulting in a remarkable hole doping effect at the

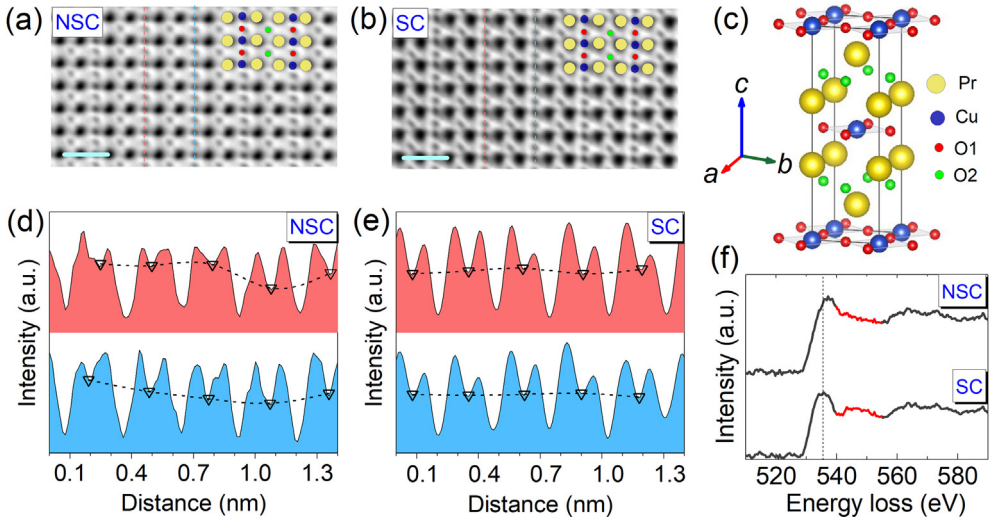

Fig. 4. (Color online) STEM and EELS study of PCO films. (a, b) Angular bright field images of NSC (a) and SC (b) samples, along the [1 1 0] zone axis. The images have been processed by averaging multiple frames with the SmartAlign software. The dark spots represent different atoms, as indicated by the model overlaid on the upper right corner, and the corresponding atom notations are shown in panel (c). Scale bar: 0.5 nm. (c) Schematic illustration of the crystal structure of $Pr_2CuO_{4\pm\delta}$. (d, e) The line profiles of CuO_2 layers in the corresponding atomic columns marked by the dashed lines in (a) and (b), respectively. The deeper valley signifies higher occupancy of oxygen or copper. The valleys marked with inverted triangle symbols represent oxygen atom positions. (f) EELS profiles of SC and NSC samples normalized to the main peak of oxygen *K* edge. The difference of the curves for SC and NSC samples is highlighted by red color.

surface and thereby allowing the emergence of superconductivity. This scenario is rather charming since hole-doped superconductor is achieved from the prototype of electron-doped cuprate superconductor [50]. Further study is desired to pinpoint the underlying mechanism of this unusual phenomenon induced by the NGV gating procedure. Nevertheless, the repair of CuO_2 plane is the key to realize non-volatile superconductivity.

4. Conclusion

In summary, we find that two different states of superconductivity can be effectively induced in insulating ternary copper oxide $Pr_2CuO_{4\pm\delta}$ by employing the ILG technique. One is volatile, resulting from electron carrier doping with PGV. The other is non-volatile, due to the replenishing of oxygen vacancies in the CuO_2 planes with NGV. Our findings provide a new paradigm for inducing and manipulating superconductivity in copper oxide superconductors, which could lead to a more detailed experimental exploration of fundamental physics as well as a route to optimize high-T_c superconductors for practical applications. Furthermore, an inexpensive and easy-to-implement method to control oxygen vacancies with several volts gate bias is technically extendable to other oxygen-sensitive functional materials.

Conflict of interest

The authors declare that they have no conflict of interest.

Acknowledgments

We thank Q. Li, G. He, X. Zhang and F. C. Zhang for fruitful discussions. This work was supported by the National Key Basic Research Program of China (2015CB921000, 2016YFA0300301, 2017YFA0302902, 2017YFA0303003 and 2018YFB0704102), the National Natural Science Foundation of China (11674374 and 11834016), the Strategic Priority Research Program of Chinese Academy of Sciences (XDB25000000), the Key Research Program of Frontier Sciences, CAS (QYZDB-SSW-SLH008 and QYZDY-SSW-SLH001), and CAS Interdisciplinary Innovation Team. This work has benefited from the bilateral collaboration F.R.S.-FNRS/NSFC (V4/345-DeM-229).

Author contributions

Kui Jin and Qihong Chen conceived the project. Xinjian Wei and Li Xu prepared the samples guided by Kui Jin and Yuan Lin. Xinjian Wei and Hao-Bo Li performed transport measurements under the guidance of Kui Jin, Qihong Chen, and Pu Yu. Qinghua Zhang and Lin Gu performed the STEM measurements. Tao Xiang provided theoretical explanation. Kui Jin, Qihong Chen and Xinjian Wei analyzed the data and wrote the paper under the assistance of all the authors.

Appendix A. Supplementary materials

Supplementary materials to this article can be found online at https://doi.org/10.1016/j.scib.2020.05.013.

References

[1] Armitage NP, Fournier P, Greene RL. Progress and perspectives on electron-doped cuprates. Rev Mod Phys 2010;82:2421–87.
[2] Keimer B, Kivelson SA, Norman MR, et al. From quantum matter to high-temperature superconductivity in copper oxides. Nature 2015;518:179–86.
[3] Jin K, Butch NP, Kirshenbaum K, et al. Link between spin fluctuations and electron pairing in copper oxide superconductors. Nature 2011;476:73–5.
[4] Bozovic I, He X, Wu J, et al. Dependence of the critical temperature in overdoped copper oxides on superfluid density. Nature 2016;536:309–11.
[5] Baumans XDA, Lombardo J, Brisbois J, et al. Healing effect of controlled anti-electromigration on conventional and high-T_c superconducting nanowires. Small 2017;13:1700384.
[6] Kang HJ, Dai P, Campbell BJ, et al. Microscopic annealing process and its impact on superconductivity in T'-structure electron-doped copper oxides. Nat Mater 2007;6:224–9.
[7] Motoyama EM, Yu G, Vishik IM, et al. Spin correlations in the electron-doped high-transition-temperature superconductor $Nd_{2-x}Ce_xCuo_{4\pm\delta}$. Nature 2007;445:186–9.
[8] Matsumoto O, Utsuki A, Tsukada A, et al. Superconductivity in undoped T'-Re_2CuO_4 with T_c over 30 K. Physica C 2008;468:1148–51.
[9] Ueno K, Nakamura S, Shimotani H, et al. Electric-field-induced superconductivity in an insulator. Nat Mater 2008;7:855–8.
[10] Yuan H, Shimotani H, Tsukazaki A, et al. High-density carrier accumulation in ZnO field-effect transistors gated by electric double layers of ionic liquids. Adv Funct Mater 2009;19:1046–53.
[11] Scherwitzl R, Zubko P, Lezama IG, et al. Electric-field control of the metal-insulator transition in ultrathin $NdNiO_3$ films. Adv Mater 2010;22:5517–20.
[12] Hwang HY, Iwasa Y, Kawasaki M, et al. Emergent phenomena at oxide interfaces. Nat Mater 2012;11:103–13.
[13] Bisri SZ, Shimizu S, Nakano M, et al. Endeavor of iontronics: from fundamentals to applications of ion-controlled electronics. Adv Mater 2017;29:1607054.
[14] Chen Q, Lu J, Liang L, et al. Continuous low-bias switching of superconductivity in a MoS_2 transistor. Adv Mater 2018;30:1800399.
[15] Ye JT, Inoue S, Kobayashi K, et al. Liquid-gated interface superconductivity on an atomically flat film. Nat Mater 2010;9:125–8.
[16] Ye JT, Zhang YJ, Akashi R, et al. Superconducting dome in a gate-tuned band insulator. Science 2012;338:1193–6.
[17] Bollinger AT, Dubuis G, Yoon J, et al. Superconductor–insulator transition in $La_{2-x}Sr_xCuO_4$ at the pair quantum resistance. Nature 2011;472:458–60.
[18] Leng X, Garcia-Barriocanal J, Bose S, et al. Electrostatic control of the evolution from a superconducting phase to an insulating phase in ultrathin $YBa_2Cu_3O_{7-x}$ films. Phys Rev Lett 2011;107:027001.
[19] Zeng SW, Huang Z, Lv WM, et al. Two-dimensional superconductor-insulator quantum phase transitions in an electron-doped cuprate. Phys Rev B 2015;92:020503(R).
[20] Zhang L, Zeng S, Yin X, et al. The mechanism of electrolyte gating on high-T_c cuprates: the role of oxygen migration and electrostatics. ACS Nano 2017;11:9950–6.
[21] Matsuoka H, Nakano M, Uchida M, et al. Signatures of charge-order correlations in transport properties of electron-doped cuprate superconductors. Phys Rev B 2018;98:144506.
[22] Lei B, Cui JH, Xiang ZJ, et al. Evolution of high-temperature superconductivity from a low-T_c phase tuned by carrier concentration in FeSe thin flakes. Phys Rev Lett 2016;116:077002.
[23] Lu N, Zhang P, Zhang Q, et al. Electric-field control of tri-state phase transformation with a selective dual-ion switch. Nature 2017;546:124–8.
[24] Jeong J, Aetukuri N, Graf T, et al. Suppression of metal-insulator transition in VO_2 by electric field–induced oxygen vacancy formation. Science 2013;339:1402–5.
[25] Li M, Han W, Jiang X, et al. Suppression of ionic liquid gate-induced metallization of $SrTiO_3$ (001) by oxygen. Nano Lett 2013;13:4675–8.
[26] Dubuis G, Yacoby Y, Zhou H, et al. Oxygen displacement in cuprates under ionic liquid field-effect gating. Sci Rep 2016;6:32378.
[27] Fête A, Rossi L, Augieri A, et al. Ionic liquid gating of ultra-thin $YBa_2Cu_3O_{7-x}$ films. Appl Phys Lett 2016;109:192601.
[28] Perez-Munoz AM, Schio P, Poloni R, et al. In operando evidence of deoxygenation in ionic liquid gating of $YBa_2Cu_3O_{7-x}$. Proc Natl Acad Sci USA 2017;114:215–20.
[29] Cui Y, Zhang G, Li H, et al. Protonation induced high-T_c phases in iron-based superconductors evidenced by NMR and magnetization measurements. Sci Bull 2018;63:11–6.
[30] He G, Wei X, Zhang X, et al. Normal-state gap in the parent cuprate $Pr_2CuO_{4\pm\delta}$. Phys Rev B 2017;96:104518.
[31] Matsumoto O, Utsuki A, Tsukada A, et al. Synthesis and properties of superconducting $T'-R_2CuO_4$ (R=Pr, Nd, Sm, Eu, Gd). Phys Rev B 2009;79:100508.
[32] Wei X, He G, Hu W, et al. Tunable superconductivity in parent cuprate $Pr_2CuO_{4\pm\delta}$ thin films. Chin Phys B 2019;28:057401.
[33] Dagan Y, Qazilbash MM, Hill CP, et al. Evidence for a quantum phase transition in $Pr_{2-x}Ce_xCuO_{4-\delta}$ from transport measurements. Phys Rev Lett 2004;92:167001.
[34] Li P, Balakirev FF, Greene RL. High-field hall resistivity and magnetoresistance of electron-doped $Pr_{2-x}Ce_xCuO_{4-\delta}$. Phys Rev Lett 2007;99:047003.
[35] Kinney J, Garcia-Barriocanal J, Goldman AM. Homes scaling in ionic liquid gated La_2CuO_{4+x} thin films. Phys Rev B 2015;92:100505.
[36] Wang M, Shen S, Ni J, et al. Electric-field-controlled phase transformation in WO_3 thin films through hydrogen evolution. Adv Mater 2017;29:1703628.
[37] Wang M, Sui X, Wang Y, et al. Manipulate the electronic and magnetic states in $NiCo_2O_4$ films through electric-field-induced protonation at elevated temperature. Adv Mater 2019;31:1900458.
[38] Rafique M, Feng Z, Lin Z, et al. Ionic liquid gating induced protonation of electron-doped cuprate superconductors. Nano Lett 2019;19:7775–80.

[39] Radaelli PG, Jorgensen JD, Schultz AJ, et al. Evidence of apical oxygen in Nd_2CuO_y determined by single-crystal neutron diffraction. Phys Rev B 1994;49:15322–6.
[40] Schultz AJ, Jorgensen JD, Peng JL, et al. Single-crystal neutron-diffraction structures of reduced and oxygenated $Nd_{2-x}Ce_xCuO_y$. Phys Rev B 1996;53:5157–9.
[41] Yuan H, Shimotani H, Ye J, et al. Electrostatic and electrochemical nature of liquid-gated electric-double-layer transistors based on oxide semiconductors. J Am Chem Soc 2010;132:18402–7.
[42] Shiogai J, Ito Y, Mitsuhashi T, et al. Electric-field-induced superconductivity in electrochemically etched ultrathin fese films on $SrTiO_3$ and MgO. Nat Phys 2015;12:42–6.
[43] Lewys J, Sigurd W, Magnus N, et al. Optimising multi-frame ADF-STEM for high-precision atomic-resolution strain mapping. Ultramicroscopy 2017;179:57–62.
[44] Taguchi M, Chainani A, Horiba K, et al. Evidence for suppressed screening on the surface of high temperature $La_{2-x}Sr_xCuO_{4-\delta}$ and $Nd_{2-x}Ce_xCuO_4$ superconductors. Phys Rev Lett 2005;95:177002.
[45] Fournier P, Mohanty P, Maiser E, et al. Insulator-metal crossover near optimal doping in $Pr_{2-x}Ce_xCuO_4$: anomalous normal-state low temperature resistivity. Phys Rev Lett 1998;81:4720–3.
[46] Damascelli A, Hussain Z, Shen Z-X. Angle-resolved photoemission studies of the cuprate superconductors. Rev Mod Phys 2003;75:473–541.
[47] Wang NL, Li G, Wu D, et al. Doping evolution of the chemical potential, spin-correlation gap, and charge dynamics of $Nd_{2-x}Ce_xCuO_4$. Phys Rev B 2006;73:184502.
[48] Jin K, Hu W, Zhu B, et al. Evolution of electronic states in n-type copper oxide superconductor via electric double layer gating. Sci Rep 2016;6:26642.
[49] Xiang T, Luo HG, Lu DH, et al. Intrinsic electron and hole bands in electron-doped cuprate superconductors. Phys Rev B 2009;79:014524.
[50] Hirsch JE. Superconductivity. The true colors of cuprates. Science 2002;295:2226–7.

Xinjian Wei obtained his B.S. degree in Applied Physics from the Anhui University in 2012, received his M.S. degree from the High Magnetic Field Laboratory, Chinese Academy of Sciences (CAS) in 2015 and obtained his Ph.D. degree in Physics under the supervision of Prof. Kui Jin at the Institute of Physics (IOP), CAS in 2019. His current research interest focuses on superconductivity, magnetism, and other novel quantum transport properties of 2D materials.

Qihong Chen obtained his Ph.D. degree in Condensed Matter Physics in 2017 under a joint program between the University of Groningen and the Hong Kong University of Science and Technology. In 2019, he joined the IOP, CAS as a faculty member. His current research interest includes the investigation of the quantum transport properties of two-dimensional layered materials and superconducting thin films using ionic gating.

Kui Jin obtained his Ph.D. degree in Physics from the IOP, CAS in 2008. From 2008 to 2012, he was a postdoc in the University of Maryland, College Park, USA. He started his research career in IOP and leads a group in the National Laboratory for Superconductivity. He has been engaged in the investigation of novel superconductivity via single crystalline films and the development of high-throughput experimentation.